NATIONAL ADVISORY COMMITTEE FOR AERONAUTICS

TECHNICAL NOTE 3670

DETERMINATION OF VORTEX PATHS BY SERIES EXPANSION TECHNIQUE WITH APPLICATION TO CRUCIFORM WINGS

By Alberta Y. Alksne

Ames Aeronautical Laboratory
Moffett Field, Calif.

Washington
April 1956

NATIONAL ADVISORY COMMITTEE FOR AERONAUTICS

TECHNICAL NOTE 3670

DETERMINATION OF VORTEX PATHS BY SERIES EXPANSION TECHNIQUE WITH APPLICATION TO CRUCIFORM WINGS

By Alberta Y. Alksne

SUMMARY

A series method of determining two-dimensional vortex paths is considered and applied to the computation of vortex positions behind a slender equal-span cruciform wing at any angle of bank as a function of the distance behind the trailing edge. Calculated paths are shown for four bank angles. For a bank angle of 45° comparison is made with the results of a closed expression given in NACA TN 2605. For other bank angles water-tank experiments provide qualitative comparison. Satisfactory agreement is found for a sufficient distance downstream to include most practical missile-tail positions.

The interference forces on an equal-span interdigitated cruciform tail behind a slender equal-span cruciform wing are calculated for four angles of bank from the vortex positions found by use of the series.

INTRODUCTION

It is now well established that the vortex wake at the tail of a slender configuration similar to those used for many missiles is often entirely rolled up and that the downwash field at the tail can be obtained by use of a single discrete vortex as an approximation to the vortex wake trailing from each wing panel. If attention is confined to configurations for which the ideas of conventional slender-body theory can be used, the problem of determining the steady-state vortex paths becomes an exact analog of the classical problem of the motion of a system of parallel rectilinear vortices.

Sacks, in reference 1, has investigated the case of an equal-span cruciform wing at 45° angle of bank where the symmetry of the problem permits the writing of a closed analytic solution for the vortex paths. The direct extension of his method to other angles of bank where no such symmetry exists does not appear feasible.

In the present paper, in order to avoid the requirement of symmetry, a series has been developed to define the vortex paths. Paths computed by this method are compared with the analytic results of Sacks for 45° angle of bank, and with the results of water-tank experiments for three other bank angles. Calculations are made of the forces on a tail due to vortices in the computed positions.

SYMBOLS

A	aspect ratio, $\frac{(2s)^2}{S}$
a	one half the distance, at $t = 0$, between the two vortices associated with a component wing[1]
b	distance of a vortex from the plane of symmetry of a component tail[1]
c	maximum chord
C_L	lift coefficient, $\frac{L}{\frac{\rho_\infty U_\infty^2}{2} S}$ (The reference area used in this report is the area of one component wing.)
C_{L_I}	interference lift coefficient (approximate)
C_{N_I}	interference normal-force coefficient
H	tail surface that is horizontal at $\phi = \frac{\pi}{4}$ for interdigitated tail
h	perpendicular distance from a vortex to a component tail
L	lift, force in the z direction
L_w	force in the z direction on a cruciform wing (invariant with bank angle)
L_I	projection of the interference normal force on the x,z plane (approximately the interference lift)
N_I	interference normal force, that is, normal force on a component tail due to the presence of vortices
n	positive integer
R	radius of a cylindrical boundary; specifically, the radius of the water tank
r	$\sqrt{(y_i - y_j)^2 + (z_i - z_j)^2}$
S	area (The reference area used in this report is the area of one component wing.)

[1]By "component wing" (or "component tail") is meant a wing (or tail) consisting of two "panels" lying in the same plane.

s	semispan at trailing edge (maximum semispan)
T	parameter used in series, $\frac{\Gamma_w t}{4\pi a^2}$
t	time, related to x by $x = U_\infty t$
U_∞	free-stream velocity
V	tail surface that is vertical at $\phi = \frac{\pi}{4}$ for interdigitated tail
v,w	velocity components in y and z directions due to two-dimensional vortices
W	complex velocity, $v - iw$
x,y,z	Cartesian coordinates, origin at center of wing trailing edge, x axis in the stream direction (See fig. 1.)
α	angle of attack, radians
$\tilde{\alpha}$	attitude angle of cruciform wing, that is, the angle between the free stream and the center line, radians
Γ	circulation, positive counterclockwise
Γ_w	reference vortex strength, invariant with bank angle, $\frac{L_w}{\rho_\infty U_\infty (2a)}$
ζ	complex coordinate, $y + iz$
$\bar{\zeta}$	$y - iz$
ρ_∞	mass density of air at free-stream conditions
τ	parameter used in series, $\frac{T}{\sqrt{2}}$
φ	perturbation velocity potential
ϕ	wing angle of bank positive clockwise

Subscripts

t	tail
w	wing

ANALYSIS

Axis System

The coordinate system used in this report is a wind-axis system as shown in figure 1, where the origin lies at the trailing edge of the wing center line. The angle of attack is required by the limitation of the theory to be small and the trailing edges of the wing panels are assumed to lie in the $x = 0$ plane.

Series Solution for Vortex Motions

Analytical solutions for the motion of a system of parallel rectilinear vortices are given by Gröbli in reference 2 for the case of three vortices with certain restrictions on the starting positions and strengths, for four vortices with a plane of symmetry, and for $2n$ vortices with n planes of symmetry. The solution for four vortices as given by Gröbli contains an error[2] but is given correctly by Sacks in reference 1 and is there applied to the case of the vortices behind a slender equal-span cruciform wing at 45° angle of bank, that is, to four vortices of equal strength starting in the form of a square. The solution in this case depends on the existence of a plane of symmetry and cannot readily be extended to cases of arbitrary vortex strength where the symmetry is lacking.

The present analysis undertakes to define the positions of a number of vortices of given strengths and initial positions in terms of a Taylor's series in powers of the time, t, thereby eliminating the dependence on symmetry. Expansion around $t = 0$ results in the following expression for the position of the i^{th} vortex:

$$\left.\begin{aligned} y_i &= (y_i)_{t=0} + \left(\frac{dy_i}{dt}\right)_{t=0} t + \left(\frac{d^2y_i}{dt^2}\right)_{t=0} \frac{t^2}{2} + \cdots \left(\frac{d^ny_i}{dt^n}\right)_{t=0} \frac{t^n}{n!} + \cdots \\ z_i &= (z_i)_{t=0} + \left(\frac{dz_i}{dt}\right)_{t=0} t + \left(\frac{d^2z_i}{dt^2}\right)_{t=0} \frac{t^2}{2} + \cdots \left(\frac{d^nz_i}{dt^n}\right)_{t=0} \frac{t^n}{n!} + \cdots \end{aligned}\right\} \quad (1)$$

The coefficients of this series can be determined by using the Biot-Savart law for two-dimensional vortices parallel to the x axis. For a system of free vortices, if v_i and w_i are the y and z components of the velocity of the i^{th} vortex due to a vortex of strength Γ_j situated at y_j, z_j, the required vortex laws are:

[2]Page 147 of reference 2, equations 23 and 24.

$$\left.\begin{aligned} v_i(t) &= \frac{d}{dt} y_i(t) = \sum_{j \neq i} \frac{-\Gamma_j}{2\pi} \frac{z_i(t) - z_j(t)}{r^2} \\ w_i(t) &= \frac{d}{dt} z_i(t) = \sum_{j \neq i} \frac{\Gamma_j}{2\pi} \frac{y_i(t) - y_j(t)}{r^2} \end{aligned}\right\} \tag{2}$$

where $r^2 = [y_i(t) - y_j(t)]^2 + [z_i(t) - z_j(t)]^2$

Now if the positions of all the vortices are known at $t = 0$, it is possible to write the coefficient of the first power of t in equation (1) for all the vortices concerned by simply substituting the initial positions into equation (2) to get $\left(\frac{dy_i}{dt}\right)_{t=0}$ and $\left(\frac{dz_i}{dt}\right)_{t=0}$. Thus the first two terms of the series are known for all the vortices, that is, y_i and z_i can now be written as linear functions of t. Substituting these first two terms into equation (2) and differentiating with respect to t and then setting t equal to zero gives the coefficient of the second power of t. Now three terms of the series are available for substitution into equation (2), etc. Note that at each step the unknown terms of the series are of no significance in the process since they still contain t as a factor after the differentiation and therefore disappear when t is set to zero.

The following formula for differentiation of a product of two functions is convenient for use in obtaining higher order terms:

$$\frac{d^n}{dt^n}\left[f(t)g(t)\right] = f\frac{d^n}{dt^n}g + \frac{n}{1!}\frac{d}{dt}f\frac{d^{n-1}}{dt^{n-1}}g + \frac{n(n-1)}{2!}\frac{d^2}{dt^2}f\frac{d^{n-2}}{dt^{n-2}}g + \cdots + \frac{n!}{(n-k)!k!}\frac{d^{n-k}}{dt^{n-k}}g\frac{d^k}{dt^k}f + \cdots + g\frac{d^n}{dt^n}f \tag{3}$$

$$n \geq 1$$

$$0 \leq k \leq n$$

In the present case, if $f(t) = \frac{1}{r^2}$ then $g(t)$ represents $(z_i - z_j)$

when $\frac{d^n}{dt^n} v_i = \frac{d^{n+1} y_i}{dt^{n+1}} = \sum_{j \neq i} \frac{-\Gamma_j}{2\pi} \frac{d^n}{dt^n} \frac{z_i - z_j}{r^2}$ is required, and $(y_i - y_j)$

when $\frac{d^n}{dt^n} w_i = \frac{d^{n+1}}{dt^{n+1}} z_i = \sum_{j \neq i} \frac{\Gamma_j}{2\pi} \frac{d^n}{dt^n} \frac{y_i - y_j}{r^2}$ is sought.

Now it can be seen that if the positions can actually be described by such a series, the only restriction on problems to be solved is that the series should converge rapidly enough to be practical for the desired values of t and that the work of evaluating the coefficients should not be prohibitive.

As a test of the method the coefficients have been determined out to the fourth power of t for the case which corresponds to the equal-span cruciform wing at any angle of bank, that is for four vortices initially placed at the corners of a square with diagonally opposite vortices of equal strength but opposite sense. Furthermore, since there was a closed analytic solution available for this configuration at an angle of bank of 45°, five additional coefficients were found for that case with a view to increased understanding of the behavior of the series.

Initial Positions and Strengths of Vortices

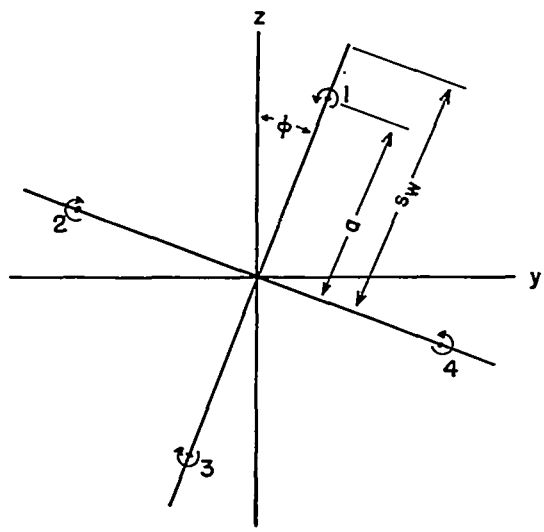

Sketch (a)

In accordance with the work of Spreiter and Sacks (ref. 3) all of the vorticity behind a wing has been assumed to be concentrated in vortex lines springing from the centroid-of-vorticity positions at the trailing edge and subject thereafter to the two-dimensional vortex laws. Since the circulation, Γ, is equal to the jump in potential, $\Delta\varphi$, and since slender-body theory leads to an elliptic spanwise distribution of $\Delta\varphi$, the centroid of vorticity at the trailing edge of each wing panel lies at a point $\pi/4$ of the distance from the center line to the wing tip. Thus, each vortex pair has a span of $2a$, where $a = (\pi/4)s_w$ as shown in sketch (a).

The lift of the equal-span cruciform wing, L_W, that is, the force in the direction of the positive z axis does not vary with angle of bank but remains throughout:

$$L_W = \rho_\infty U_\infty \Gamma_W (2a) \tag{4}$$

where Γ_W is the circulation around the horizontal wing at angle of bank $\phi = 0$. At other angles of bank the vortex strengths are related to Γ_W as follows:

$$\left.\begin{aligned} \Gamma_4 = -\Gamma_2 = \Gamma_W \cos \phi \\ \Gamma_1 = -\Gamma_3 = \Gamma_W \sin \phi \end{aligned}\right\} \tag{5}$$

where the vortices are numbered as in sketch (a).

Solutions

The use of equations (1), (2), (3), and (5), together with the fact that the initial positions of the vortices are known in terms of the wing semispan, s_W, and the bank angle, ϕ, leads to a series for the vortex positions at any time t. Coefficients have been found out to the fourth power of t, and with the substitution

$$T = \frac{\Gamma_W t}{4\pi a^2} \tag{6}$$

the series can be written as follows:

$$
\begin{aligned}
\frac{4y_1}{\pi s_w} &= \sin\phi - (\sin\phi\cos\phi)T - \frac{2}{3}(\sin\phi\cos^3\phi)T^3 + \\
&\quad \frac{2}{3}(\sin\phi\cos^2\phi)(\sin^2\phi - \cos^2\phi)T^4 \ldots \\
\\
\frac{4z_1}{\pi s_w} &= \cos\phi - (1 + \cos^2\phi)T - (\cos\phi)T^2 - \frac{1}{3}\cos^2\phi(1 + 2\cos^2\phi)T^3 - \\
&\quad \frac{1}{3}\cos\phi(3 - 4\sin^2\phi\cos^2\phi)T^4 \ldots \\
\\
\frac{4y_2}{\pi s_w} &= -\cos\phi + (\sin\phi\cos\phi)T + \frac{2}{3}(\sin^3\phi\cos\phi)T^3 + \\
&\quad \frac{2}{3}(\sin^2\phi\cos\phi)(\sin^2\phi - \cos^2\phi)T^4 \ldots \\
\\
\frac{4z_2}{\pi s_w} &= \sin\phi - (1 + \sin^2\phi)T - (\sin\phi)T^2 - \frac{1}{3}\sin^2\phi(1 + 2\sin^2\phi)T^3 - \\
&\quad \frac{1}{3}\sin\phi(3 - 4\sin^2\phi\cos^2\phi)T^4 \ldots \\
\\
\frac{4y_3}{\pi s_w} &= -\sin\phi - (\sin\phi\cos\phi)T - \frac{2}{3}(\sin\phi\cos^3\phi)T^3 - \\
&\quad \frac{2}{3}(\sin\phi\cos^2\phi)(\sin^2\phi - \cos^2\phi)T^4 \ldots \\
\\
\frac{4z_3}{\pi s_w} &= -\cos\phi - (1 + \cos^2\phi)T + (\cos\phi)T^2 - \frac{1}{3}\cos^2\phi(1 + 2\cos^2\phi)T^3 + \\
&\quad \frac{1}{3}\cos\phi(3 - 4\sin^2\phi\cos^2\phi)T^4 \ldots \\
\\
\frac{4y_4}{\pi s_w} &= \cos\phi + (\sin\phi\cos\phi)T + \frac{2}{3}(\sin^3\phi\cos\phi)T^3 - \\
&\quad \frac{2}{3}(\sin^2\phi\cos\phi)(\sin^2\phi - \cos^2\phi)T^4 \ldots \\
\\
\frac{4z_4}{\pi s_w} &= -\sin\phi - (1 + \sin^2\phi)T + (\sin\phi)T^2 - \frac{1}{3}\sin^2\phi(1 + 2\sin^2\phi)T^3 + \\
&\quad \frac{1}{3}\sin\phi(3 - 4\sin^2\phi\cos^2\phi)T^4 \ldots
\end{aligned}
\qquad (7)
$$

For the special case treated by Sacks, that is, the equal-span cruciform wing at an angle of bank $\phi = \pi/4$, there is a plane of symmetry and the series is simplified so that the labor of evaluating the coefficients is a great deal less. For this case coefficients were found out to the ninth power of t. Since $\cos\phi = \sin\phi = 1/\sqrt{2}$, and $\Gamma_1 = -\Gamma_3 = \Gamma_4 = -\Gamma_2 = \frac{\Gamma_w}{\sqrt{2}}$ the series can be written, letting $\tau = T/\sqrt{2}$:

$$\left.\begin{aligned}
\frac{4\sqrt{2}}{\pi}\frac{y_1}{s_w} &= 1 - \tau - \frac{2}{3}\tau^3 - \frac{8}{15}\tau^5 + \frac{134}{315}\tau^7 + \frac{13318}{2835}\tau^9 \ldots \\
\frac{4\sqrt{2}}{\pi}\frac{z_1}{s_w} &= 1 - 3\tau - 2\tau^2 - \frac{4}{3}\tau^3 - \frac{8}{3}\tau^4 - \frac{28}{15}\tau^5 - \frac{226}{45}\tau^6 - \\
&\qquad \frac{932}{315}\tau^7 - \frac{3062}{315}\tau^8 - \frac{12172}{2835}\tau^9 \ldots \\
\frac{4\sqrt{2}}{\pi}\frac{y_4}{s_w} &= 1 + \tau + \frac{2}{3}\tau^3 + \frac{8}{15}\tau^5 - \frac{134}{315}\tau^7 - \frac{13318}{2835}\tau^9 \ldots \\
\frac{4\sqrt{2}}{\pi}\frac{z_4}{s_w} &= -1 - 3\tau + 2\tau^2 - \frac{4}{3}\tau^3 + \frac{8}{3}\tau^4 - \frac{28}{15}\tau^5 + \\
&\qquad \frac{226}{45}\tau^6 - \frac{932}{315}\tau^7 + \frac{3062}{315}\tau^8 - \frac{12172}{2835}\tau^9 \ldots
\end{aligned}\right\} \quad (8)$$

Relation Between T and x

As pointed out previously, the vortex laws used here apply to straight-line vortices, parallel to the x axis, extending to infinity in both directions, and changing their position with time. Their use in the situation to which they are to be applied depends on the three-dimensional steady-state vortex picture showing relatively gradual variations in the x direction. Within the limits of slender-body theory the correspondence is exact, and the results obtained in the previous section can be used to compute the three-dimensional vortex paths behind a slender equal-span cruciform wing by means of the relation

$$x = U_\infty t \quad (9)$$

Now since

$$T = \frac{\Gamma_W t}{4\pi a^2} \tag{6}$$

and

$$L_W = \rho_\infty U_\infty \Gamma_W (2a) \tag{4}$$

and in slender theory

$$C_L = (\pi/2) A\alpha \tag{10}$$

the positions of the vortices at any downstream station, x/s_W, can be found from equation (7), or for 45° bank from equation (8), by use of the relation

$$\frac{x}{s_W} = \frac{\pi^4 (s_W)^2}{4 C_{L_W} S_W} T = \frac{\pi^3 (s_W)^2}{2 A_W S_W \bar{\alpha}_W} T \tag{11}$$

where $\bar{\alpha}_W$ is the "attitude angle," that is, the angle between the center line of the cruciform wing and the free-stream direction.

If $A_W = \frac{4 s_W}{c_W}$ as for triangular wings, then equation (11) can be written:

$$\frac{x}{s_W} = \frac{\pi^4 A_W}{16 C_{L_W}} T = \frac{\pi^3}{8 \bar{\alpha}_W} T \tag{12}$$

Equation (12) provides the relation used in the present report.

EXPERIMENT

In order to provide a qualitative means of judging the results of the computations for angles of bank for which no closed analytic solution is available, experiments were run with small models in a water tank. Water miscible paint spread on the trailing edge before each run remained floating on the surface of the water behind the model and made the vortices visible. For various reasons, it was considered inadvisable to attempt quantitative comparison. For one thing, there is no general agreement as to the point in a vortex swirl which is to be considered the center of the core, and the centroid of vorticity, which is the quantity calculated in this report, is even more difficult to define. For another thing, the best pictures were obtained at angles of attack

which were too high to be entirely compatible with the assumptions of the theory. However, the water-tank experiments were expected to demonstrate the trends in the variation of the vortex patterns with bank angle.

Water Tank and Models

The water tank used in the present experiments was the same as that described by Sacks (ref. 1) and is shown in figure 2. Three different models were used, all equal-span cruciform wings constructed of sheet metal 0.050 inch thick. One model had an 8-inch span and an aspect ratio of 2. The others were smaller, having only a 4-inch span. One of these had an aspect ratio of 1, the other, 2. Various angles of attack were tried. The most successful runs were made at $\bar{\alpha} = \frac{\pi}{12} = 15^{\circ}$. As in reference 1, motion pictures provided a record of the distance traveled by the wing as well as of the changing vortex patterns.

The water tank was not deep enough for the 8-inch-span model to continue running much beyond two span lengths below the surface. However, the camera was kept running after the model stopped and the time measured in frames was used to determine an equivalent distance.

Accuracy and Repeatability of Experimental Data

It was found that runs made with the two small models showed excessive influence of currents set up in the tank by the supporting mechanism and by various outside distrubances. The vortex paths behind the model with 8-inch span showed little effect of stray disturbances but, since the water-tank diameter was only 22 inches, there was a large systematic error due to wall interference.

A comparison was made of the vortex patterns at corresponding distances behind the three different models for $\phi = \pi/4$. The choosing of the particular runs in which the symmetrical vortex pattern typical of this symmetrical configuration was maintained eliminated most of the irrelevant disturbances which made data from the small models generally unsatisfactory. Measured in terms of the half span of the model, the y coordinates of the vortex cores at corresponding distances behind the three models did not differ by more than 10 percent. However, the z coordinates behind the large model differed from those behind the small models by about 25 percent.

A wall-interference correction consisting of a constant upwash, computed on the assumption of four discrete vortices (see Appendix A) was sufficient to bring the results for the large model into very good agreement with those for the small models. Since this was the case for

the bank angle of 45° where the general nature of the vortex pattern was known, and since the upwash at $t = 0$ was found, under the same assumption, not to vary with bank angle, it was assumed that the data obtained from the large model for other angles would also be satisfactory when the same correction was applied. The water-tank pictures shown in this report are those taken with the large-span model and the necessary corrections are indicated by additional reference points marked at the sides of the prints.

No allowance was made for the effects of stopping the model before the runs were complete. The influence, if any, should have appeared as an additional downwash at the surface near the end of a run, but none was noted in comparing runs made with the large and small models.

RESULTS AND DISCUSSION

Computations of vortex paths behind a cruciform wing have been made using equations (7) and (8) for four angles of bank, $\phi = \pi/16, \pi/8, 3\pi/16, \pi/4$. Figure 3 shows the paths with y/s_w plotted against z/s_w for various values of x/s_w in a coordinate system in which the x axis lies in the stream direction and the bank angle is measured from the z axis and is positive when the starboard wing is rotated down. The points shown are for $T = 0$, 0.276, 0.352, 0.449, 0.517, 0.582, 0.650, and 0.766, which for an aspect-ratio-2 wing with a lift coefficient of 0.82 ($\bar{\alpha} = \pi/12$), corresponds to $x/s_w = 0$, 4.1, 5.2, 6.6, 7.6, 8.6, 9.6, and 11.4; that is, this figure may be considered either as a time history or as a representation of three-dimensional vortex paths.

Computations have been carried out to a value of T corresponding to the "leapfrog" position of reference 1, that is, to the value at which the two upper vortices pass between the two lower vortices for a bank angle of 45°.

Figure 4 shows water-tank pictures taken with the 8-inch-span model at an attitude angle of $\pi/12$ radians and at bank angles of $\pi/16$, $\pi/8$, and $3\pi/16$. Choice of the appropriate frames from the motion picture film made it possible to present pictures corresponding very closely to most of the values of T used in the computations. No comparison is shown for small values of T where the vortices were in the process of rolling up and the visible vortex cores were not only poorly defined but did not yet correspond to the centroids of vorticity. As can be seen from the first picture of each series, the solid white markers indicate the point at which the trailing-edge center line entered the water. The open white markers indicate the corrected position of this reference point, shifted upward to account for the upwash due to the presence of the tank wall. (See Appendix A.) It can be seen that the variation with angle of bank found by the calculations (fig. 3) is similar to that shown in figure 4.

In figure 3(d) the positions as calculated by the formulas of reference 1 are shown for comparison with the series results at a bank angle of $\pi/4$. For this bank angle the ninth-order terms of the series were available from equation (8). Points are also shown computed with terms out to the fourth order as for the other angles of bank. Even at the "leapfrog" position (last point computed) the agreement is good if ninth-order terms are used. If only terms out to the fourth order are used, the largest error appears in the z coordinate of the fast moving vortices 1 and 2, but at a point which, for $\bar{\alpha} = 12$, would correspond to a distance downstream of four times the wing span, the error is still less than 10 percent of the total change of position in the z direction, or about 5 percent of the wing span.

From this comparison with the work of Sacks, together with the fact that the water-tank pictures for other angles of bank also show qualitative agreement with the computed vortex positions, it appears that the series computations give satisfactory results for a distance of several wing spans behind the trailing edge.

As a further check on the dependability of the series method the results for $\phi = \pi/4$ using one term of the series, two terms, three terms, etc., are presented in figures 5 and 6, again in comparison with the results calculated from the formulas of Sacks. In these figures the values of y/s_W and z/s_W are plotted separately against the parameter T, which is related to the downstream distance as in equation (12), so that

$$T = \frac{xC_{L_W}16}{s_W A_W \pi^4}$$

It can be seen from these figures that the series appears to converge quite rapidly for small values of T, and to converge, although more slowly, even for the highest value of T used. Sketch (b) shows the sum of the first n terms plotted against n, out to $n = 9$, for $T = 0.517$ for vortices 1 and 4. (The first term, $n = 0$, is not shown as it is simply the initial position.) It can be seen that in both cases the series for y/s_W converges very quickly. Note also that only the odd powers of T appear in

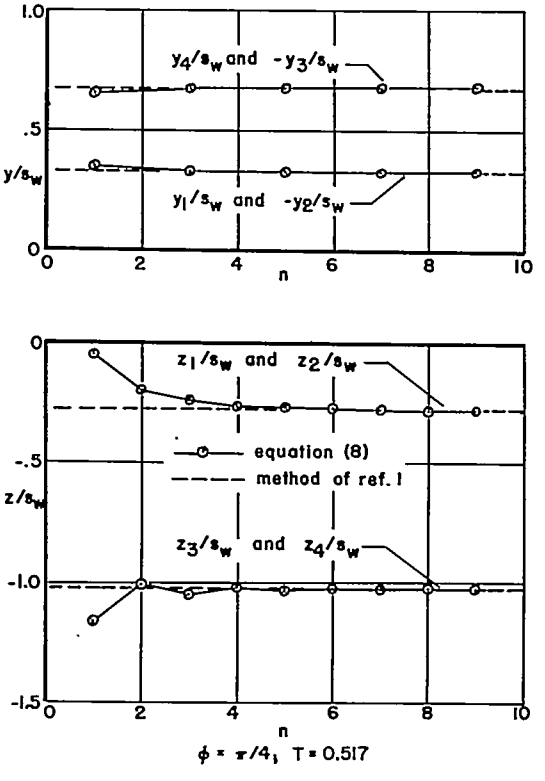

Sketch (b)

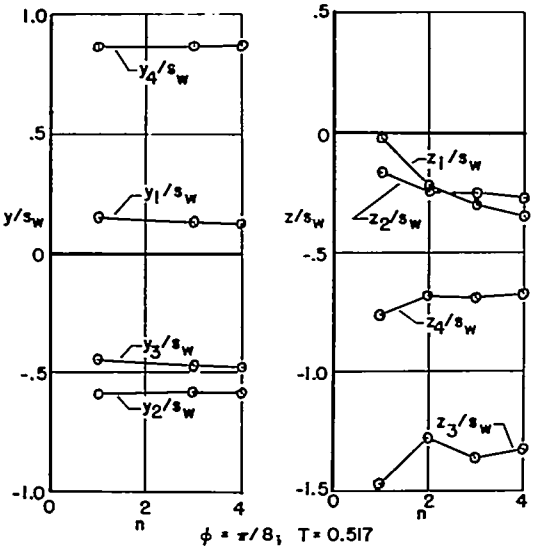

Sketch (c)

the series for y/s_w. The series for z_4/s_w alternates and that for z_1/s_w does not; however, both approach the correct value very rapidly at $T = 0.517$.

Figures 7 and 8 show y/s_w and z/s_w plotted against T for each of the four vortices for a bank angle of $\pi/8$. Only fourth-order terms are available for this case, but it can be seen that the behavior of the series is very similar to that observed for $\phi = \pi/4$. Sketch (c) shows the sum of the first n terms for $\phi = \pi/8$ plotted against n out to $n = 4$ for each vortex for $T = 0.517$, further substantiating the statement concerning similar behavior, although the convergence is slower.

It appears from these considerations that for small values of T only two or three terms of the series are required and that four terms are enough to give good results out to about $T = 0.5$. Beyond that point the results become somewhat doubtful unless more terms are used, but this provides a fairly wide range of useful values, as can be seen from the fact that for a lift coefficient of 0.5 and an aspect ratio of 2, $T = 0.5$ corresponds to about six span lengths behind the trailing edge of the wing.

CALCULATION OF LIFT ON A CRUCIFORM TAIL

The lift on the tail of a slender wing-tail combination due to the vortices from the wing can be computed by reverse flow techniques as discussed in reference 3, on the assumption that the tail does not influence the positions of the vortices. The equation

$$N_I = \Gamma \rho_\infty U_\infty s_t \left\{ -\frac{b}{s_t} + \frac{b}{|b|} \sqrt{\frac{1}{2}\left[\sqrt{\left(1 + \frac{h^2}{s_t^2} - \frac{b^2}{s_t^2}\right)^2 + \frac{4b^2h^2}{s_t^4}} - \left(1 + \frac{h^2}{s_t^2} - \frac{b^2}{s_t^2}\right) \right]} \right\} \tag{13}$$

given in reference 4 yields the normal force on a component tail, or tail plane (see sketch (d)), due to a single vortex. Note that a factor has been placed in front of the outer radical to take account of the case of $b < 0$. The effects of all the vortices must be summed for each component tail and the components of force in the z direction added to give the lift.

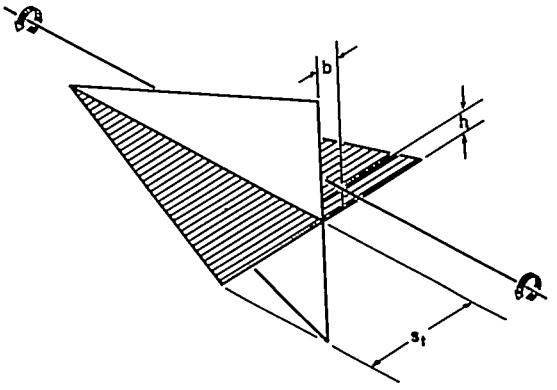

Sketch (d)

The configuration chosen for the present calculations was a cruciform tail interdigitated behind a cruciform wing as in sketch (e), where the tail components are designated V and H as shown. Note that the tail center line is an extension of the wing center line, whereas the x axis lies in the stream direction. Since no account was taken of the effect of the tail on the vortex paths, the vortex positions used in the force calculations were those already computed in the absence of a tail for the station corresponding to the tail trailing edge.

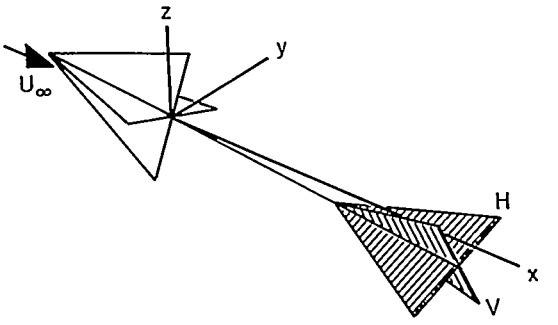

Sketch (e)

The normal-force coefficients on each tail plane have been computed from equation (13) for four angles of bank for three ratios of tail span to wing span, and for $T = 0.247$ and $T = 0.411$. It should be noticed that varying T corresponds to varying either the tail length, the wing lift coefficient, or the aspect ratio (see eq. (12)). For $C_L = 0.5$ and $A = 2$ these values of T correspond to $x/s_w = 6$ and $x/s_w = 10$. The results are shown in figure 9.

In figure 10 is shown the lift coefficient of the tail due to the presence of the vortices, that is, the interference lift coefficient, C_{L_I}, measured in the positive z direction (the same direction as the lift on the wing). It is interesting to note that for $T = 0.247$ and $s_t/s_w = 1$, and also for $T = 0.411$ and $s_t/s_w = 1.2$, there is very little variation of interference lift coefficient with angle of bank.

A comparison with analytical results obtained by the method of reference 5 for 45° angle of bank is shown in figure 11, in which the interference lift is plotted against the tail-span to wing-span ratio. The agreement is very good, as of course should be expected since the vortex positions agree so well.

CONCLUDING REMARKS

Computations of vortex paths and of forces on a tail behind a slender equal-span cruciform wing have been made using a series to determine the vortex positions as a function of the distance downstream. The results show that, for a bank angle of 45°, only a few terms of the series are needed to provide satisfactory agreement with the known analytic solution at downstream distances encompassing most practical missile tail positions. Comparison with water-tank pictures of the vortex patterns for other angles of bank, and consideration of the relative size of successive terms of the series, indicate that the same is true for the general case where no analytic solution is known.

Ames Aeronautical Laboratory
National Advisory Committee for Aeronautics
Moffett Field, Calif., Feb. 8, 1956

APPENDIX A

WALL-INTERFERENCE CORRECTIONS

As in the case of tunnel-wall corrections, the effect of surrounding a group of vortices with a solid cylindrical boundary of radius R can be calculated by the method of images when the vortex positions and strengths are known.

For each vortex within the boundary, the position is given as ζ_j where $\zeta = y + iz$ and $i = \sqrt{-1}$. The position of the image outside the boundary is then known and is $R^2/\bar{\zeta}_j$ where $\bar{\zeta} = y - iz$. Then at a point ζ the complex velocity due to the image vortex is

$$W = v - iw = \frac{\partial}{\partial \zeta}\left[\frac{i\Gamma_j}{2\pi} \ln\left(\zeta - \frac{R^2}{\bar{\zeta}_j}\right)\right] = \frac{i\Gamma_j}{2\pi\left(\zeta - \frac{R^2}{\bar{\zeta}_j}\right)} \tag{A1}$$

If the field of interest is confined to a small area in the center of the cylinder and if the vortices also remain in this area, ζ may be neglected as very small compared to $R^2/\bar{\zeta}_j$ and the complex velocity due to a number of image vortices may be written

$$W = \sum_{j=1}^{n} \frac{i(-\Gamma_j \bar{\zeta}_j)}{2\pi R^2} \tag{A2}$$

Then

$$\left.\begin{aligned} w &= \sum_{j=1}^{n} \frac{\Gamma_j}{2\pi R^2} \mathrm{IPi}\bar{\zeta}_j = \sum_{j=1}^{n} \frac{\Gamma_j y_j}{2\pi R^2} \\ v &= \sum_{j=1}^{n} \frac{(-\Gamma_j)}{2\pi R^2} \mathrm{RPi}\bar{\zeta}_j = \sum_{j=1}^{n} \frac{(-\Gamma_j z_j)}{2\pi R^2} \end{aligned}\right\} \tag{A3}$$

Since the present report is concerned with an equal-span cruciform wing, there are assumed to be only four vortices within the boundary and the relation between their strengths is

$$\left.\begin{aligned}\Gamma_1 &= -\Gamma_3 = \Gamma_w \sin \phi \\ \Gamma_4 &= -\Gamma_2 = \Gamma_w \cos \phi\end{aligned}\right\} \tag{5}$$

Then at the center of the cylinder

$$\left.\begin{aligned}w &= \frac{\Gamma_w}{2\pi R^2}\left[(y_1 - y_3)\sin \phi + (y_4 - y_2)\cos \phi\right] \\ v &= \frac{-\Gamma_w}{2\pi R^2}\left[(z_1 - z_3)\sin \phi + (z_4 - z_2)\cos \phi\right]\end{aligned}\right\} \tag{A4}$$

where y_1, y_2, y_3, y_4 and z_1, z_2, z_3, and z_4 depend on t. At $t = 0$ the positions of the vortices are known in terms of ϕ and the semispan, s_w, and the expressions for w and v simplify to

$$\left.\begin{aligned}w &= \frac{\Gamma_w s_w}{4R^2} \\ v &= 0\end{aligned}\right\} \tag{A5}$$

for any angle of bank.

For the special case of 45° bank angle, $\sin \phi = \cos \phi = \frac{1}{\sqrt{2}}$ and symmetry provides relations between the vortex positions so that

$$\left.\begin{aligned}w &= \frac{\Gamma_w}{\pi R^2 \sqrt{2}}(y_1 + y_4) \\ v &= 0\end{aligned}\right\} \tag{A6}$$

at any time t. Furthermore it is known (see refs. 1 and 2) that for this case $(y_1 + y_4)$ is constant with time so at the center of the cylinder

$$w = \text{constant}; \qquad v = 0 \tag{A7}$$

as long as symmetry with respect to the z axis is maintained.

Since, near the center of the cylinder, the upwash for all angles of bank is the same at $t = 0$ and the upwash for $\phi = \pi/4$ does not change with time, it has been assumed that one correction, namely,

$$w = \frac{\Gamma_w s_w}{4R^2}$$

could be used throughout. This resulted in a correction of $\frac{\Gamma_w s_w t}{4R^2}$ to the z position at any time, t, where R is the radius of the water tank.

REFERENCES

1. Sacks, Alvin H.: Behavior of Vortex Systems Behind Cruciform Wings - Motions of Fully Rolled-Up Vortices. NACA TN 2605, 1952.

2. Gröbli, Dr. W.: Specielle Probleme über die Bewegung geradliniger paralleler Wirbelfäden. Vierteljahrsshrift der Naturforschenden Gesellschaft in Zurich, vol. 22, 1877, pt. 1, pp. 37-81, pt. 2, pp. 129-165.

3. Spreiter, John R., and Sacks, Alvin H.: A Theoretical Study of the Aerodynamics of Slender Cruciform-Wing Arrangements and Their Wakes. NACA TN 3528, 1956.

4. Heaslet, Max. A., and Lomax, Harvard: Supersonic and Transonic Small Perturbation Theory. (Sec. D of General Theory of High Speed Aerodynamics. Vol. VI of High Speed Aerodynamics and Jet Propulsion, W. R. Sears, ed., Princeton Univ. Press, 1954.)

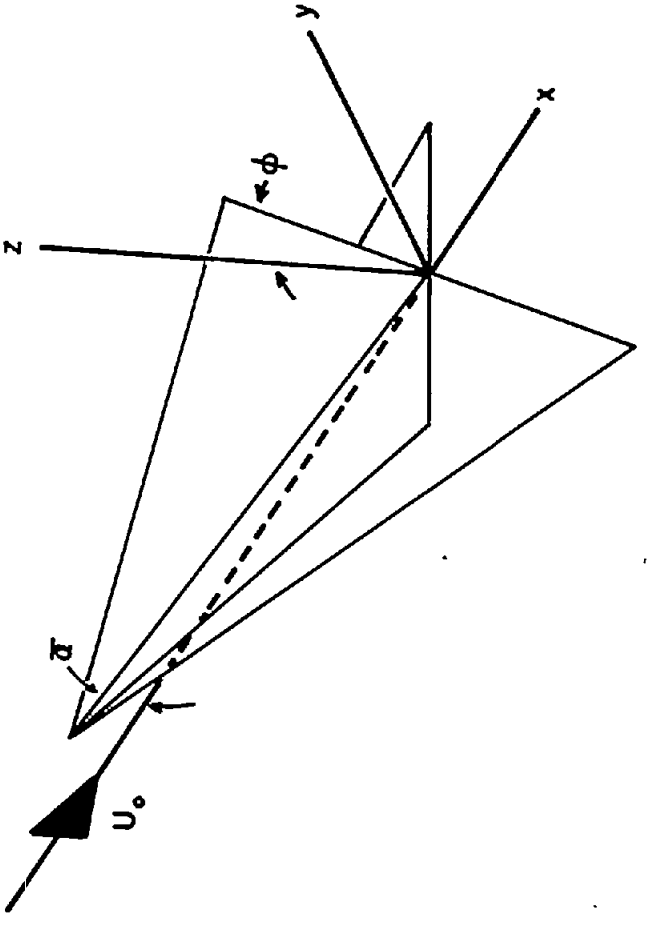

Figure 1.- Axis system.

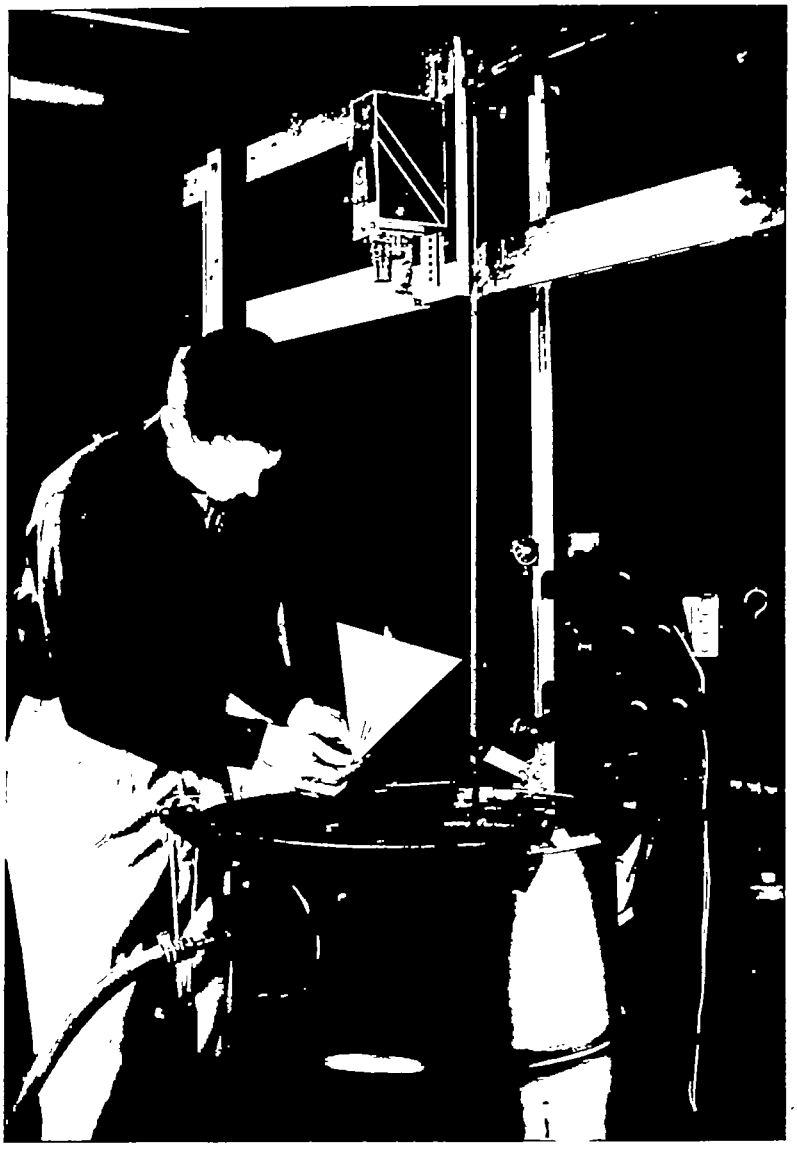

A-16303

Figure 2.- Water tank with cruciform model.

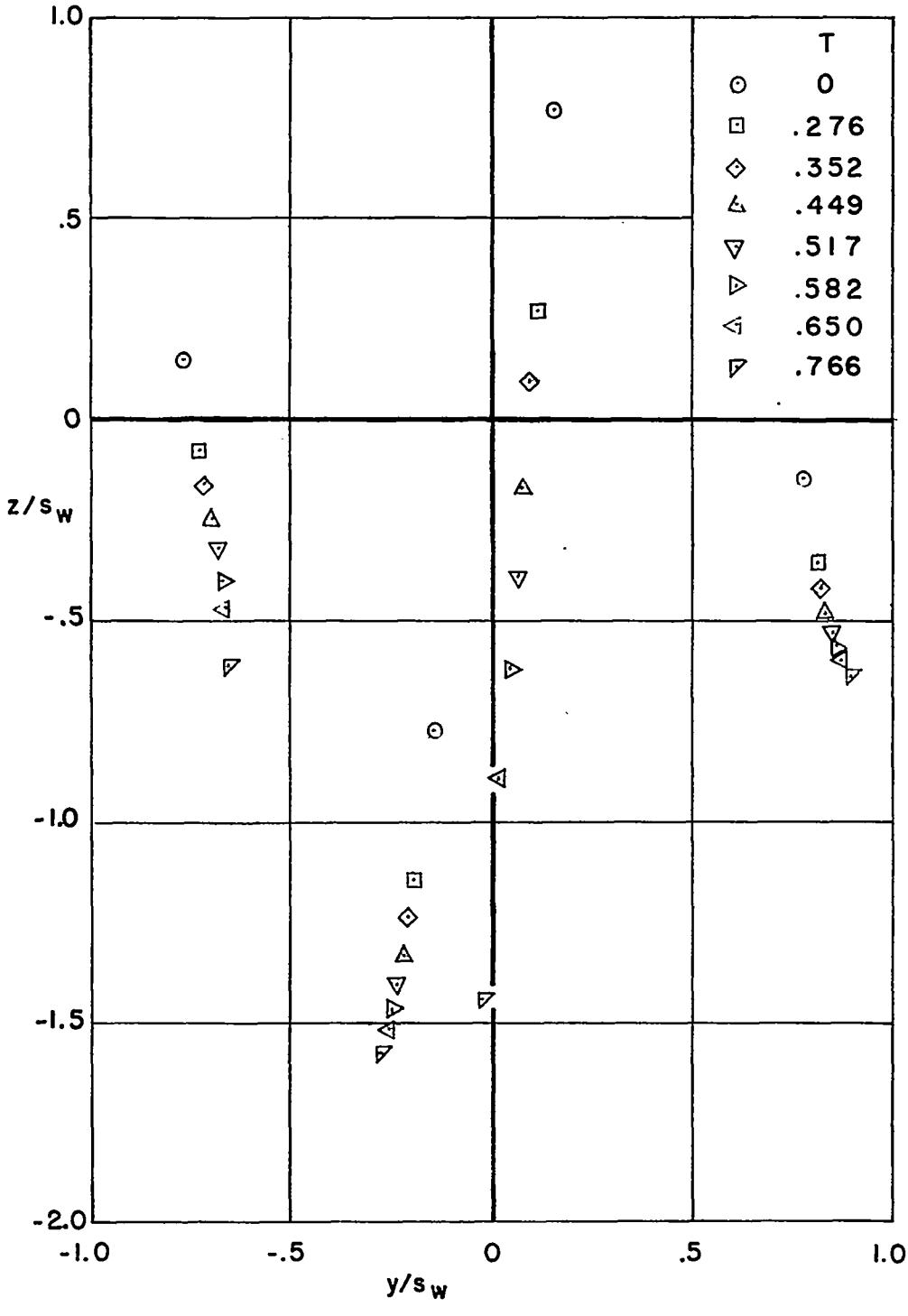

(a) $\phi = \pi/16$

Figure 3.- Vortex paths behind a cruciform wing at four different angles of bank.

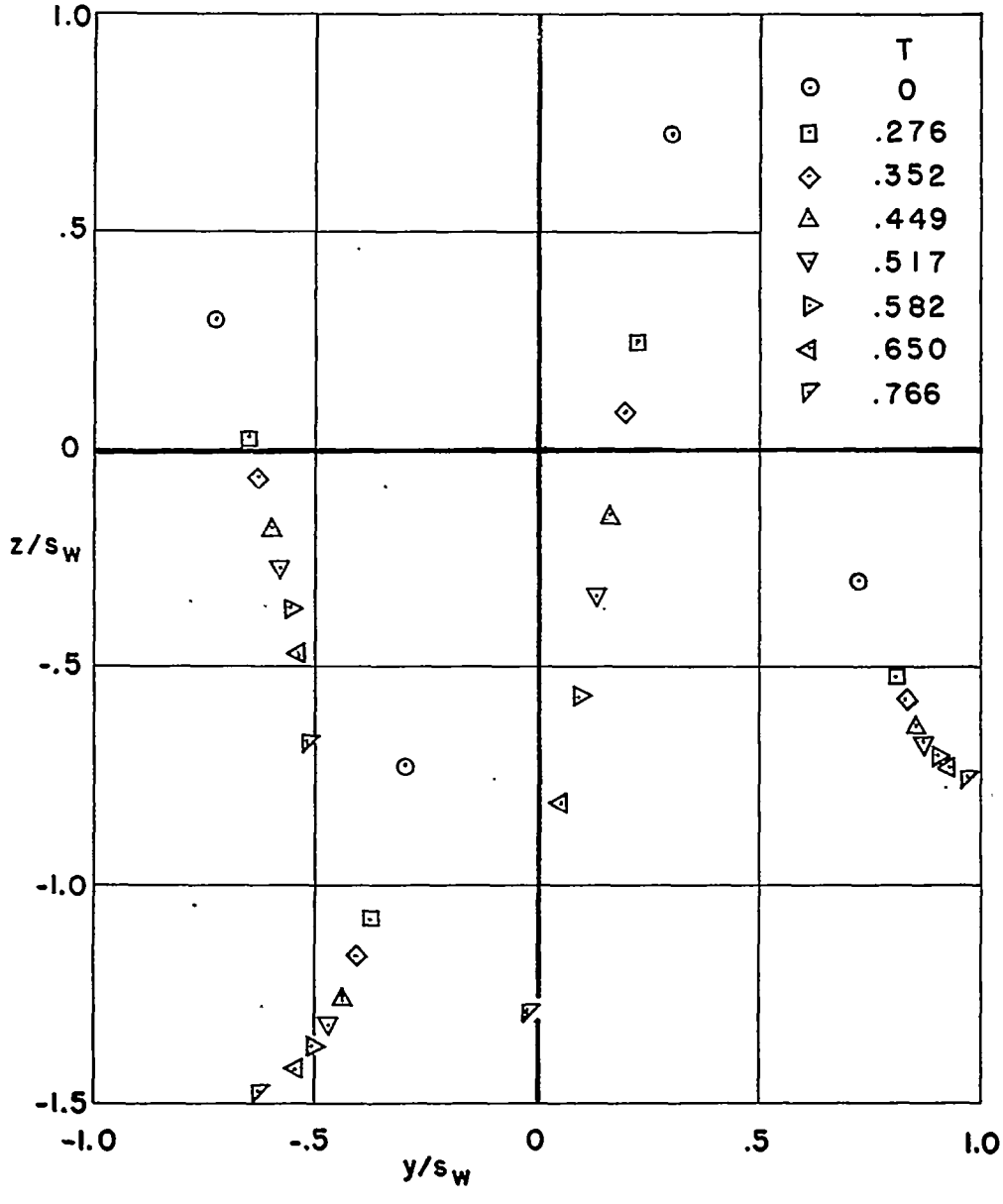

(b) $\phi = \pi/8$

Figure 3.- Continued.

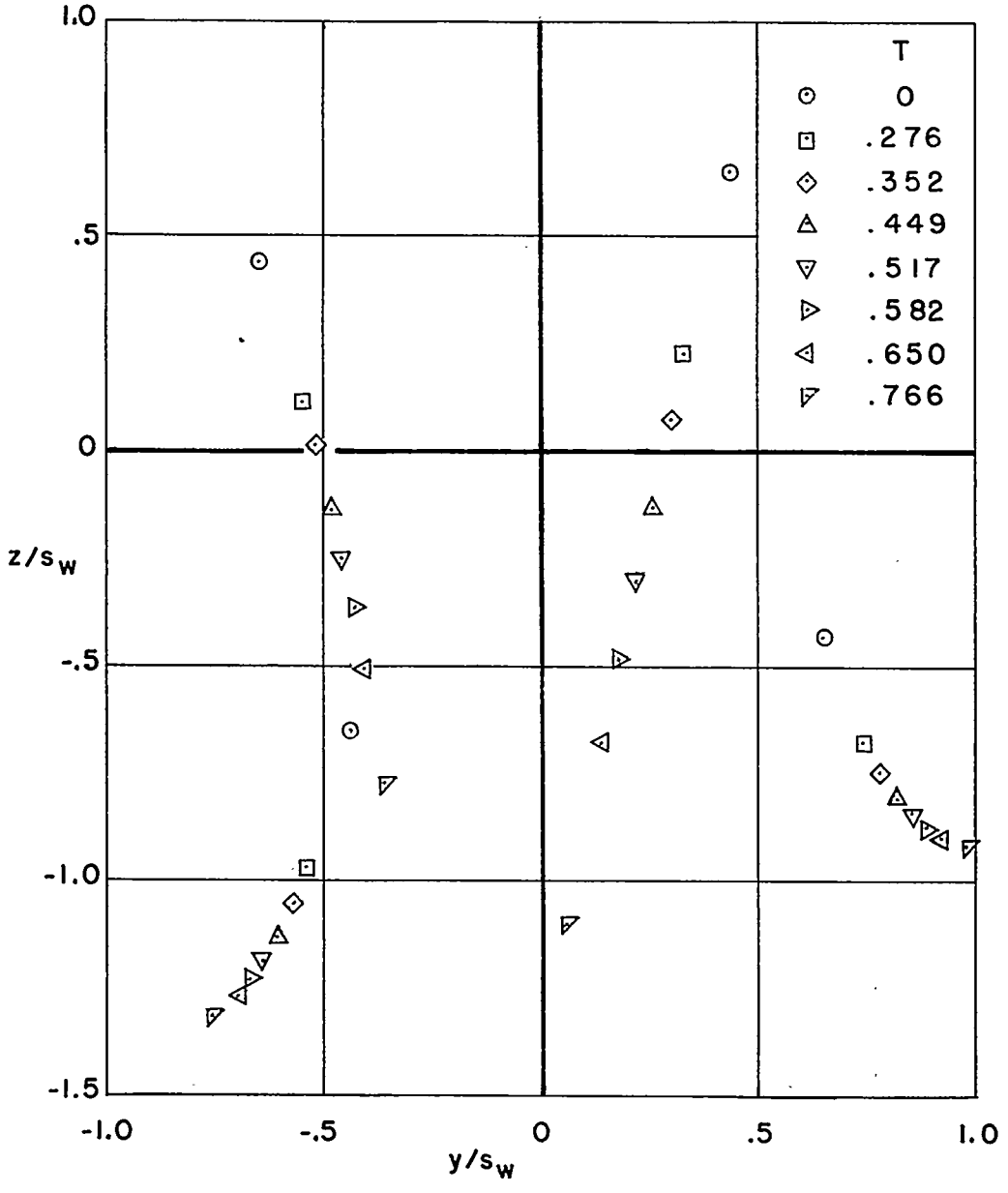

(c) $\phi = 3\pi/16$

Figure 3.- Continued.

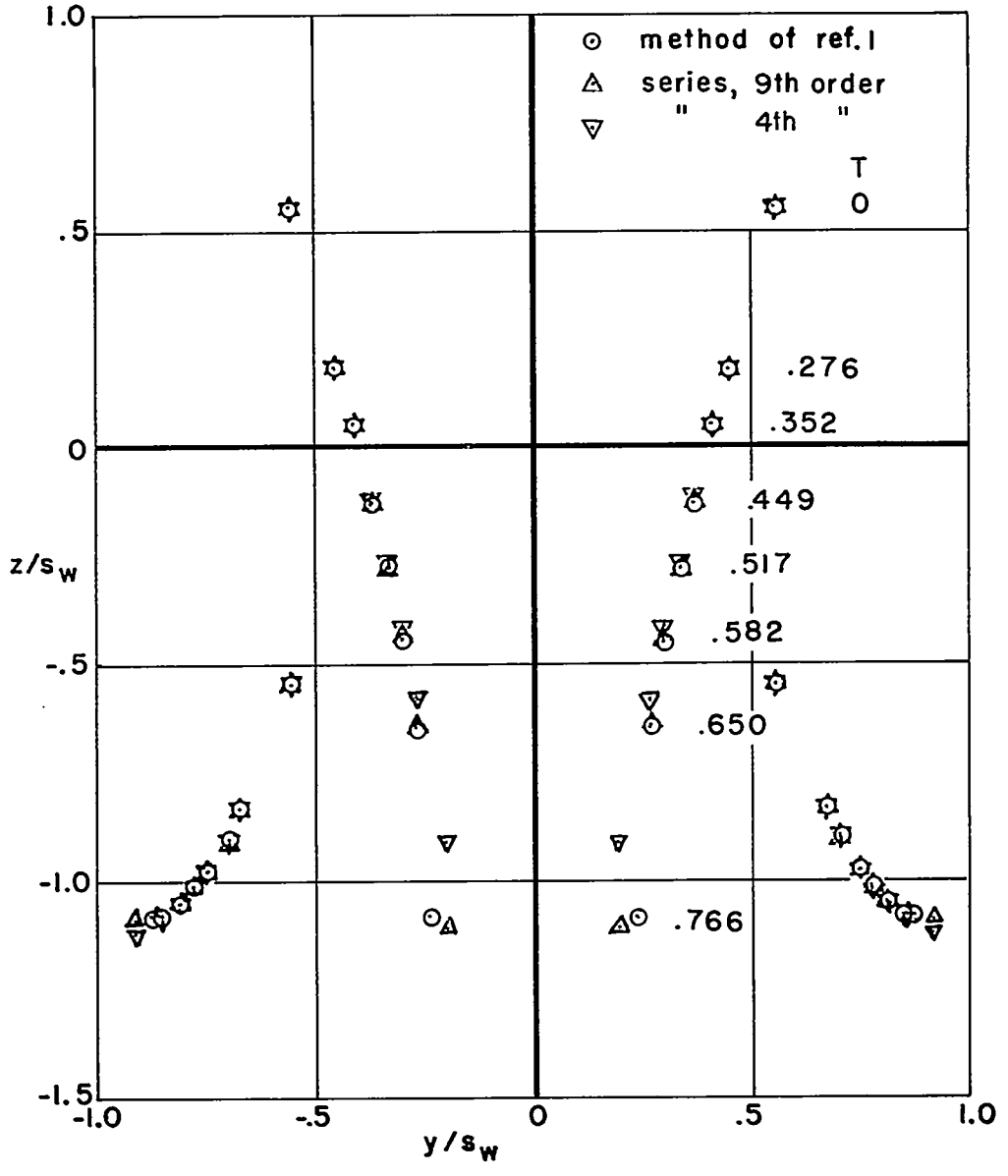

(d) $\phi = \pi/4$

Figure 3.- Concluded.

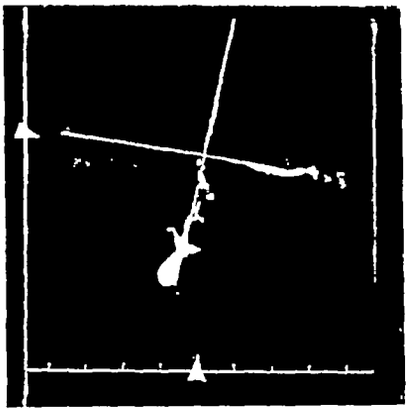

$x/s_w = 0$

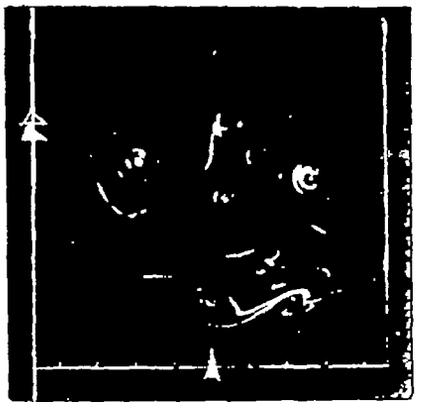

$x/s_w = 6.6$

$x/s_w = 4.1$

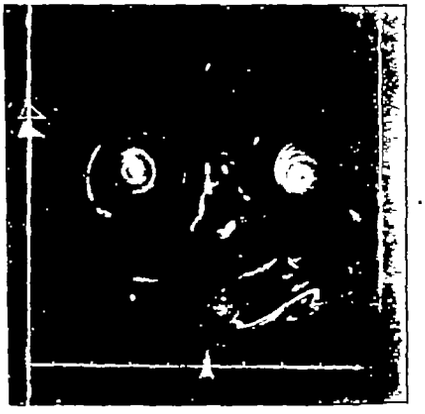

$x/s_w = 7.6$

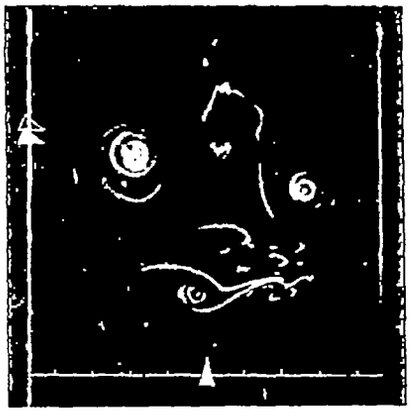

$x/s_w = 5.2$

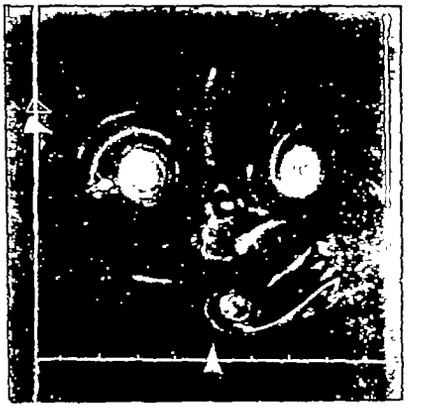

$x/s_w = 8.6$

(a) $\phi = \pi/16$

Figure 4.- Photographs of wake at various stations behind a cruciform wing of aspect ratio 2, for three different bank angles; $\bar{\alpha} = \pi/12$.

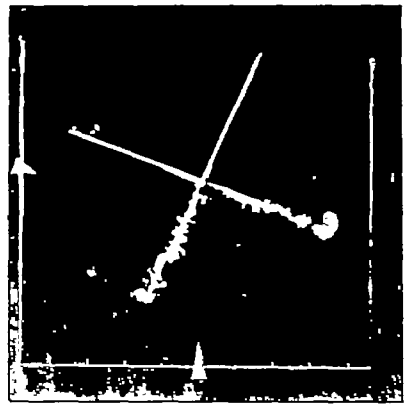

$x/s_w = 0$

$x/s_w = 6.6$

$x/s_w = 4.1$

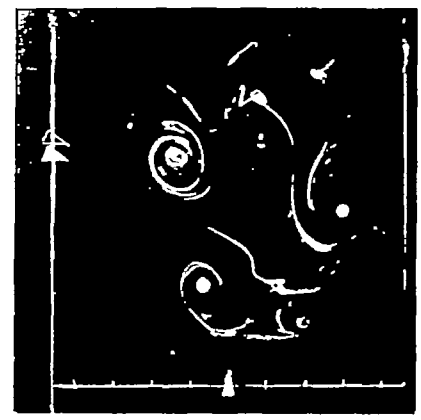

$x/s_w = 7.6$

$x/s_w = 5.2$

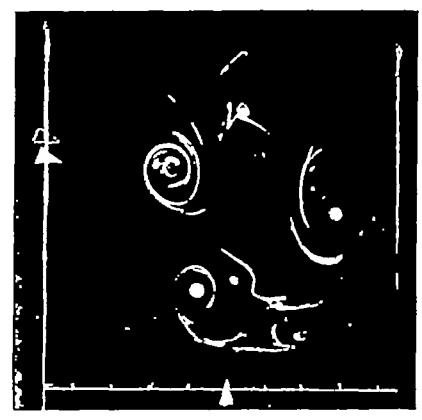

$x/s_w = 8.6$

(b) $\phi = \pi/8$

Figure 4.- Continued.

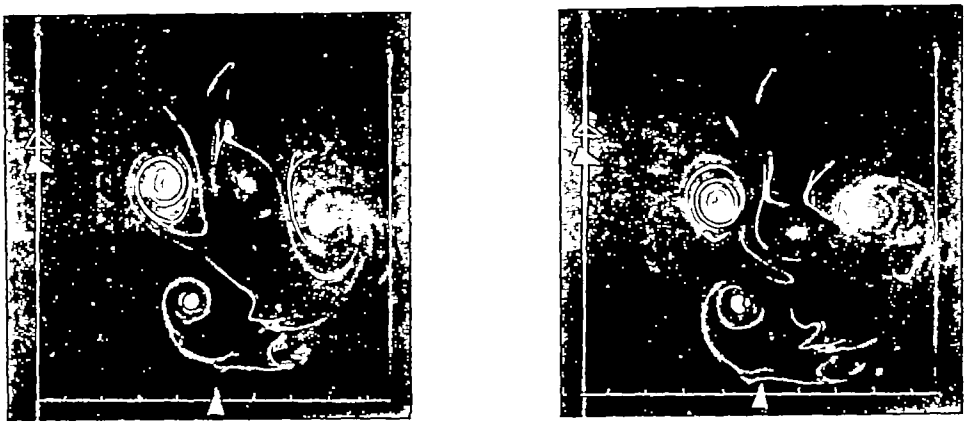

$x/s_w = 9.6$ $x/s_w = 11.4$

(b) $\phi = \pi/8$ - Concluded.

Figure 4.- Continued.

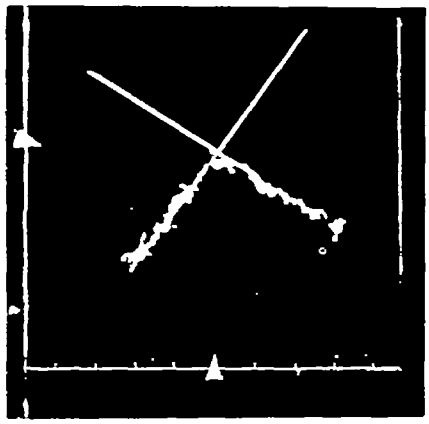

$x/s_w = 0$

$x/s_w = 6.6$

$x/s_w = 4.1$

$x/s_w = 7.6$

$x/s_w = 5.2$

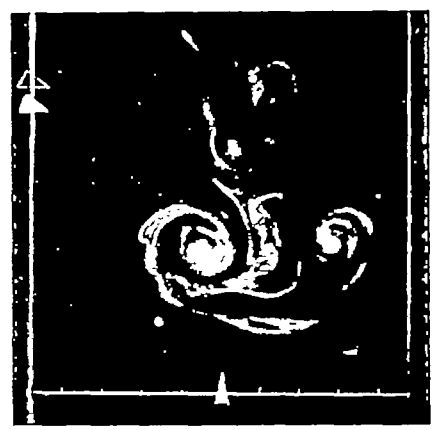

$x/s_w = 8.6$

(c) $\phi = 3\pi/16$

Figure 4.- Concluded.

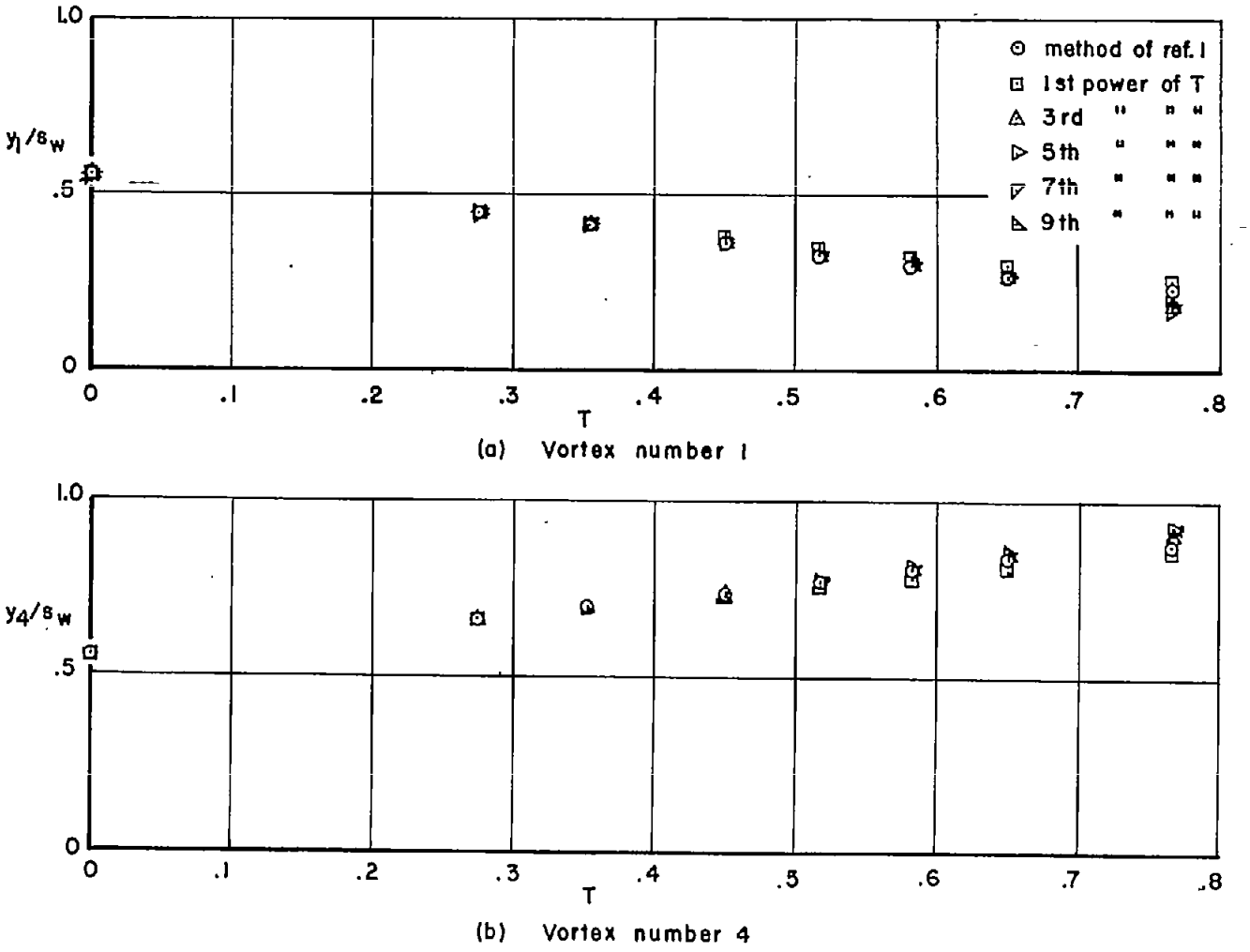

Figure 5.- Variation with the parameter T of the lateral position y/s_w of vortex 1 and vortex 4 behind a cruciform wing, calculated with one, two, three, four, etc., terms of the series; $\phi = \pi/4$.

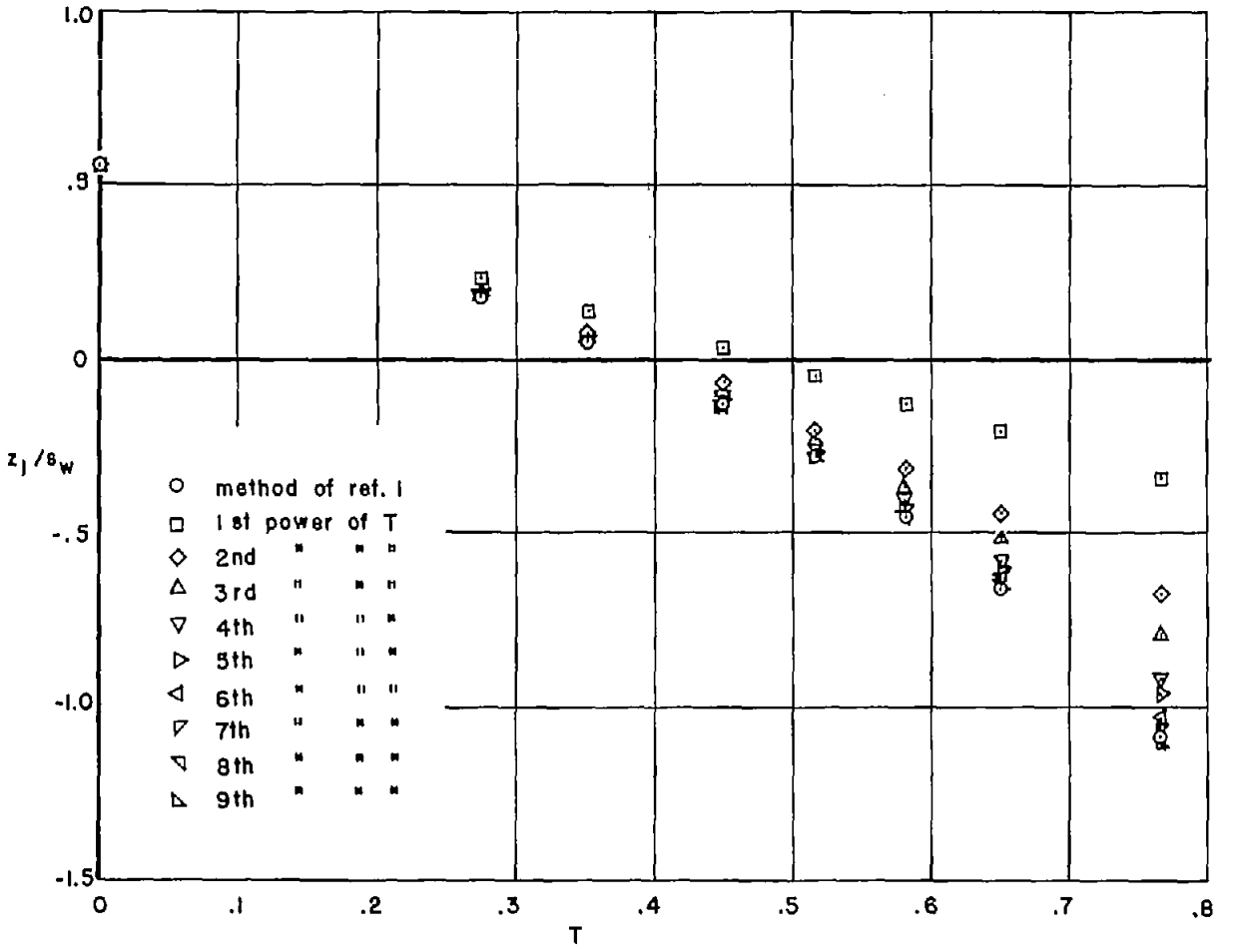

(a) Vortex number 1.

Figure 6.- Variation with the parameter T of vertical position z/s_w of vortex 1 and vortex 4 behind a cruciform wing, calculated with one, two, three, four, etc., terms of the series; $\phi = \pi/4$.

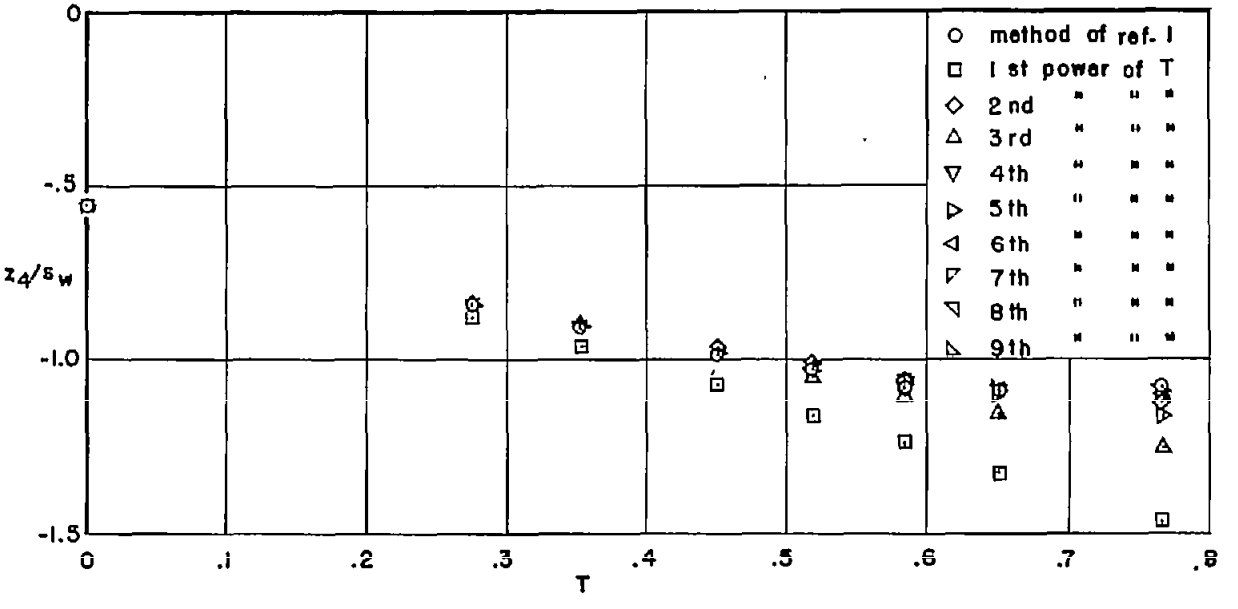

(b) Vortex number 4.

Figure 6.- Concluded.

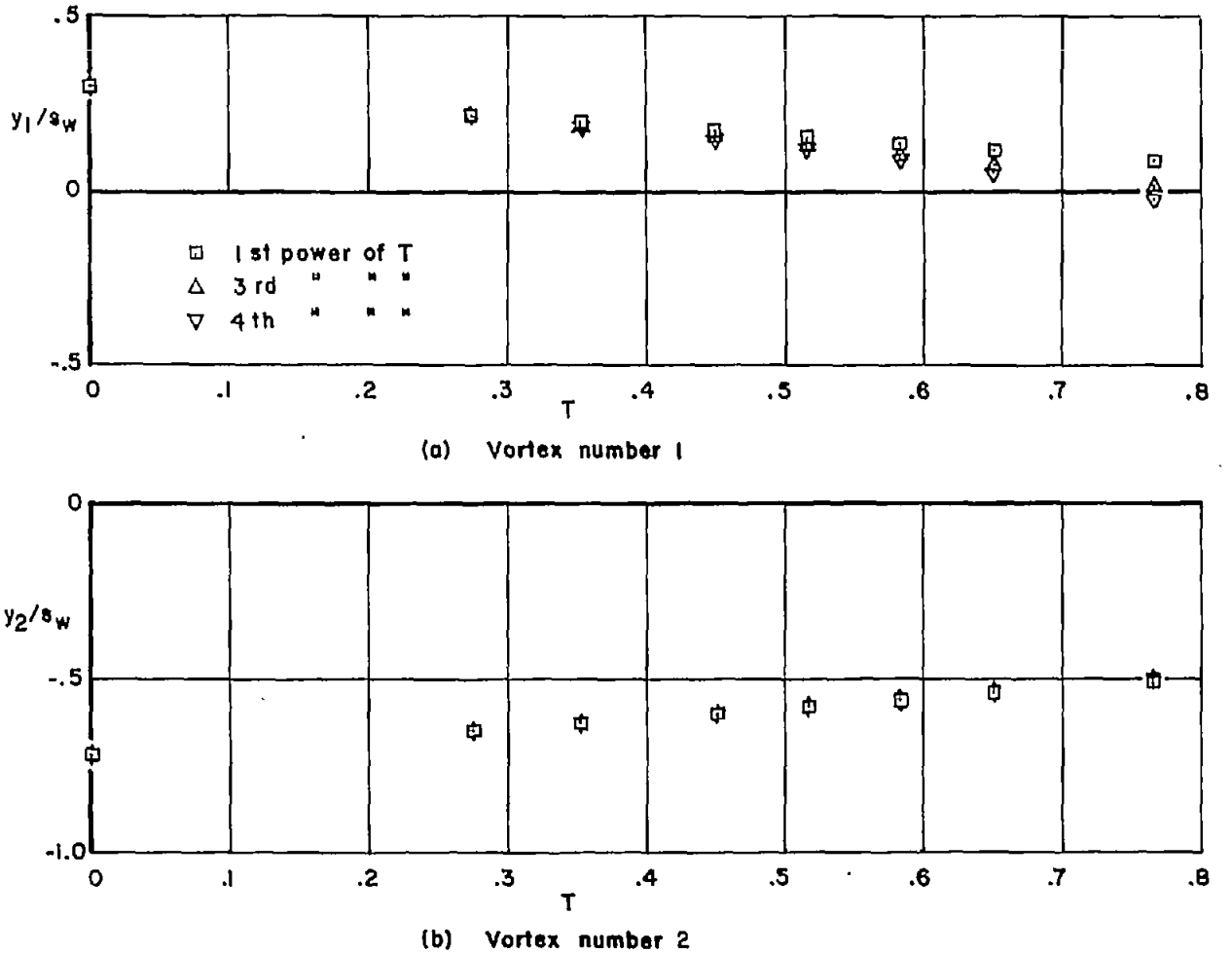

Figure 7.- Variation with the parameter T of lateral position y/s_w for each of the four vortices behind a cruciform wing, calculated with one, two, three, and four terms of the series; $\phi = \pi/8$.

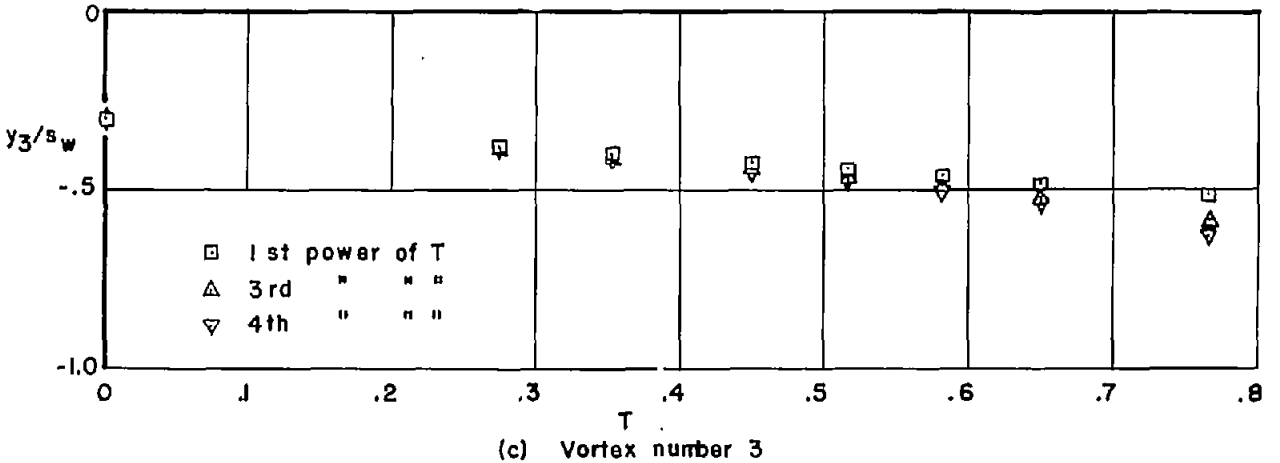

(c) Vortex number 3

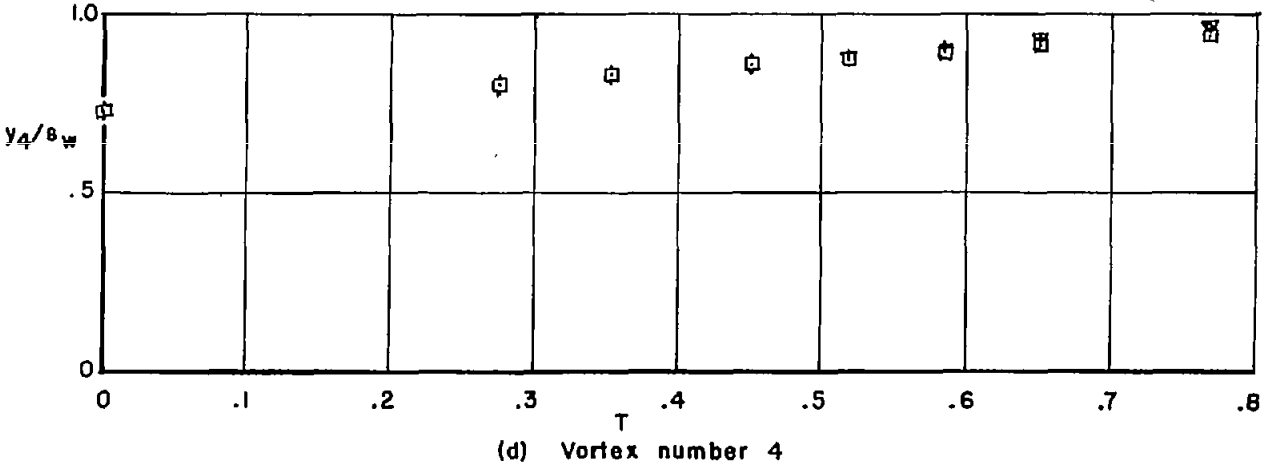

(d) Vortex number 4

Figure 7.- Concluded.

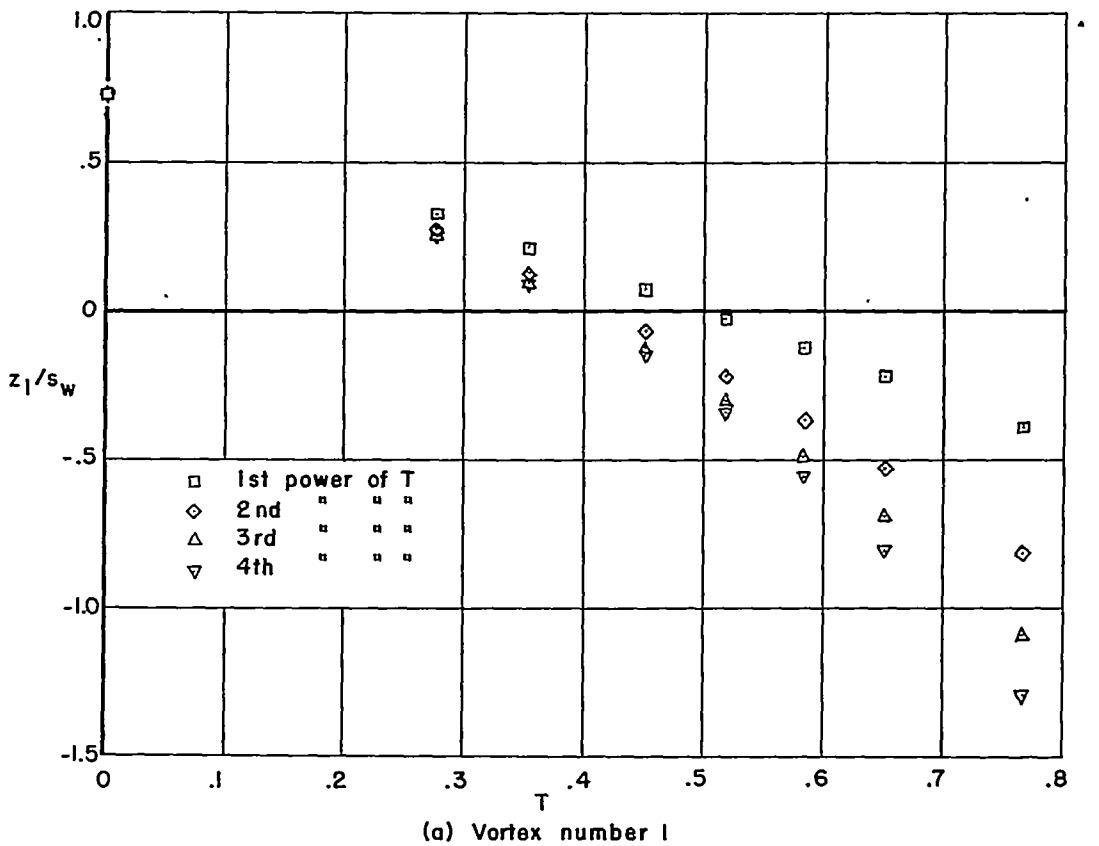

(a) Vortex number 1

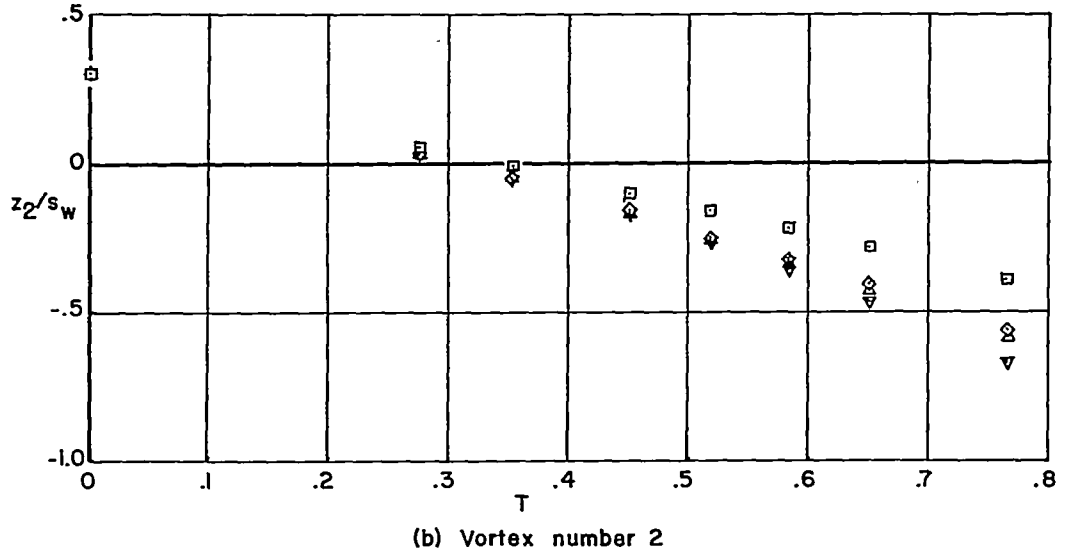

(b) Vortex number 2

Figure 8.- Variation with the parameter T of vertical position z/s_w for each of the four vortices behind a cruciform wing, calculated with one, two, three, and four terms of the series; $\phi = \pi/8$.

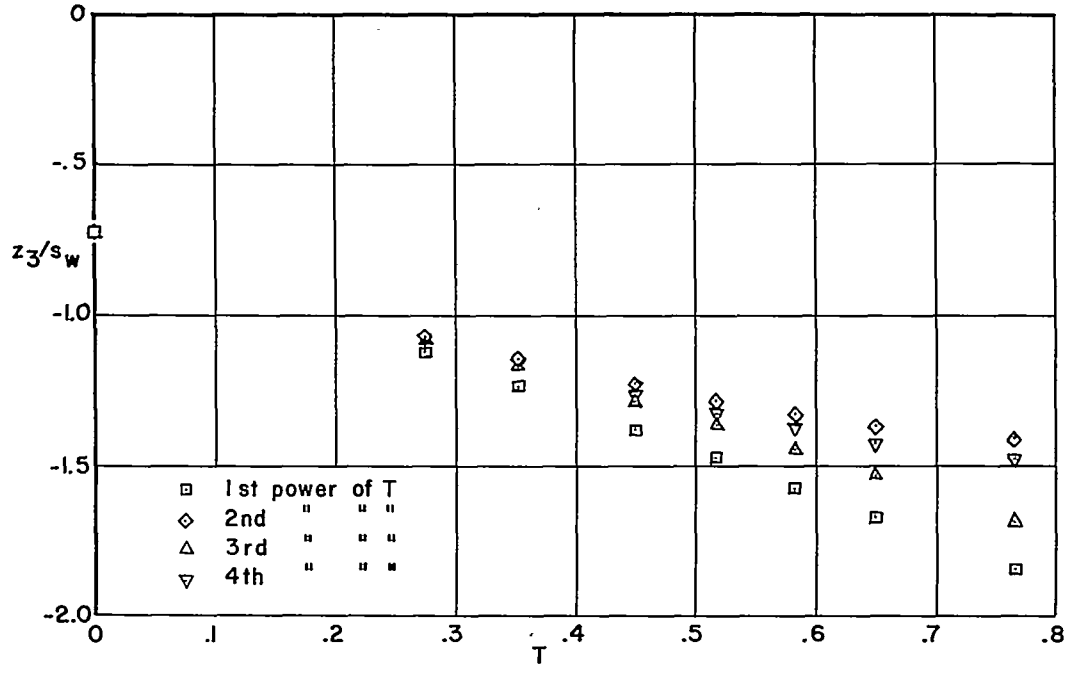

(c) Vortex number 3

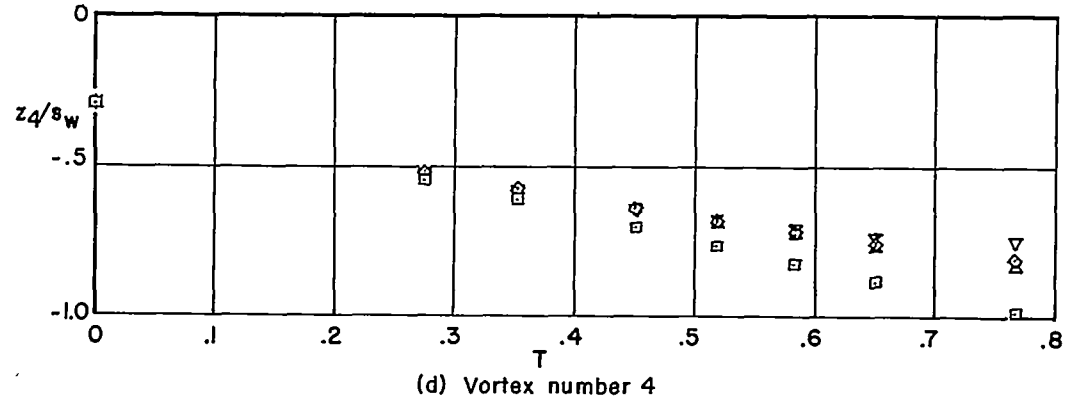

(d) Vortex number 4

Figure 8.- Concluded.

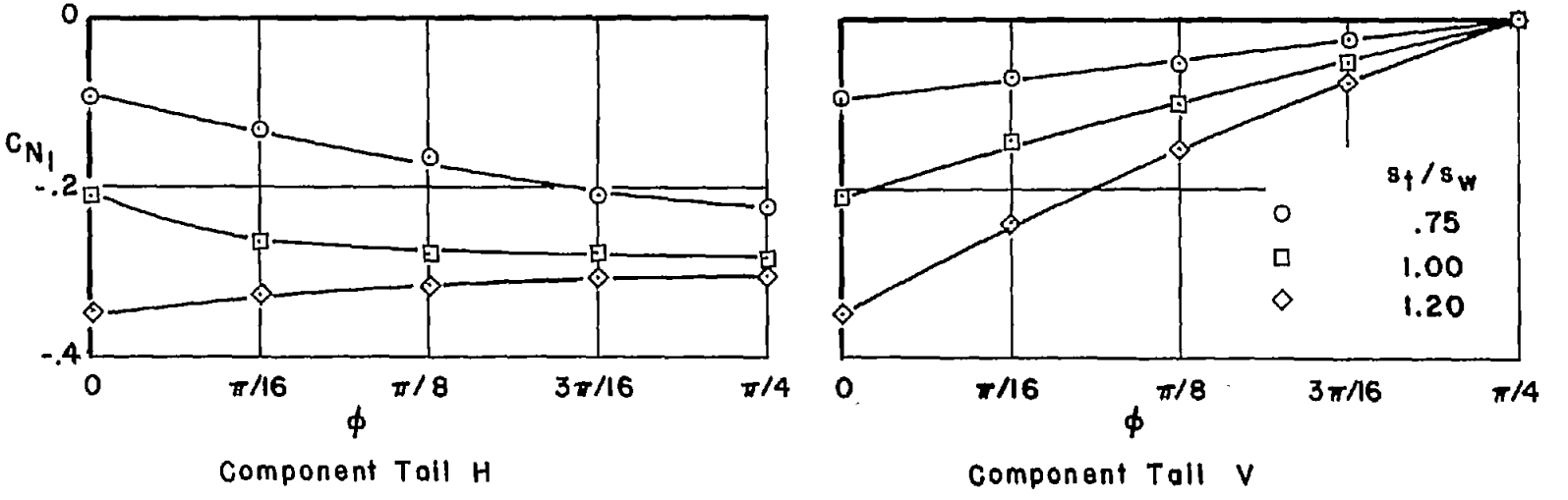

(a) T = 0.247

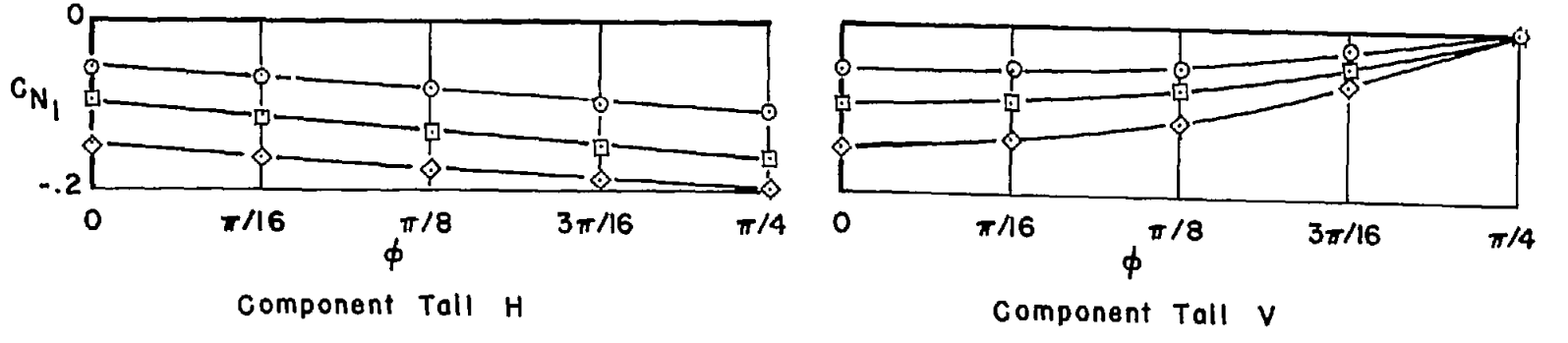

(b) T = 0.411

Figure 9.- Variation of interference normal-force coefficient C_{N_I} with bank angle ϕ for an interdigitated cruciform tail at two values of the downstream distance parameter T behind a cruciform wing.

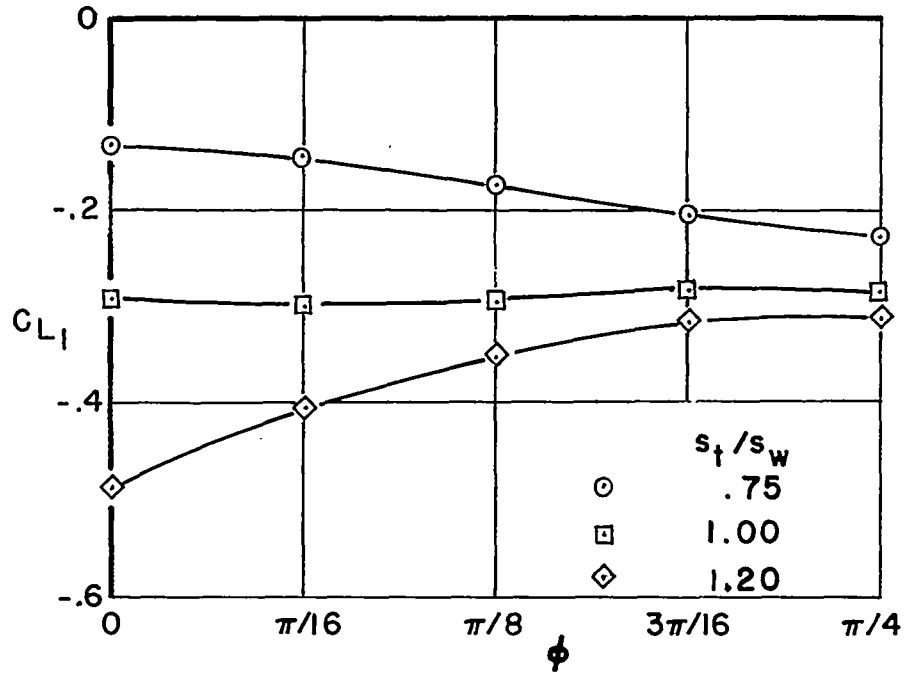

(a) T = 0.247

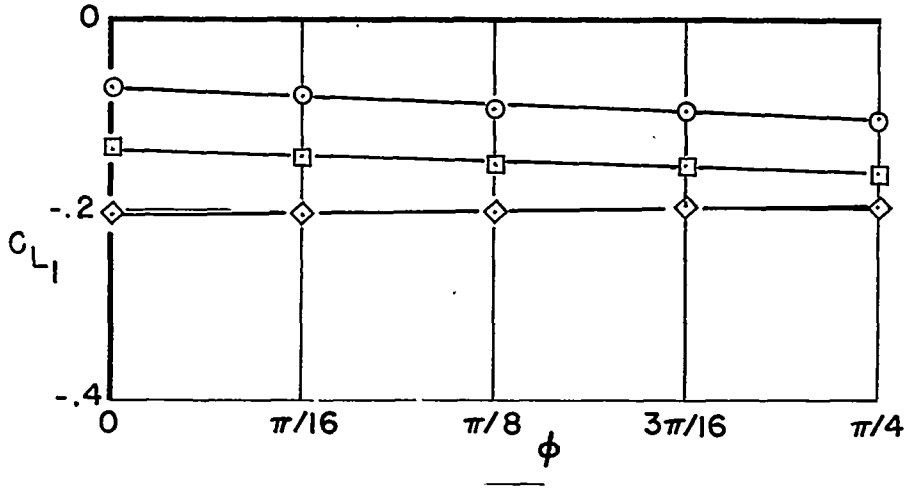

(b) T = 0.411

Figure 10.- Variation with bank angle ϕ of the interference lift coefficient C_{L_I} on an interdigitated cruciform tail at two values of the downstream distance parameter T behind a cruciform wing.

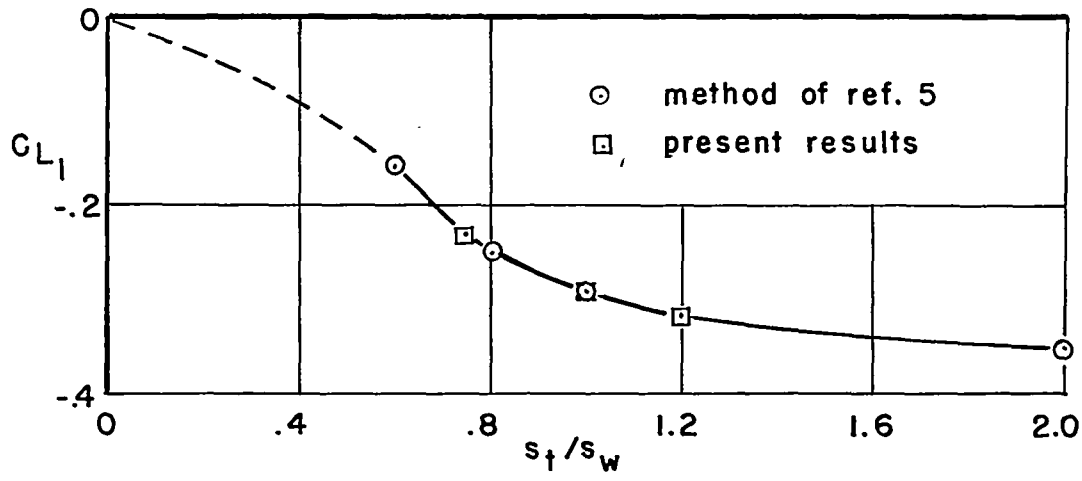

Figure 11.- Variation with the ratio of tail span to wing span of the interference lift coefficient on an interdigitated cruciform tail behind a cruciform wing at angle of bank, $\phi = \pi/4$; $C_{L_I} = 0.5$; $x/s_w = 6$.